Journal of Nuclear Medicine, published on October 14, 2021 as doi:10.2967/jnumed.121.262600

Combined PARP1-targeted nuclear contrast and reflectance contrast enhances confocal microscopic detection of basal cell carcinoma

Aditi Sahu, PhD[1], Jose Cordero, PhD[1,2], Xiancheng Wu[1,3], BS, Susanne Kossatz, PhD,[4,5,6] Ucalene Harris BS[1], Paula Demetrio Desouza Franca, MD,[4] Nicholas R. Kurtansky, BS,[1] Niasia Everett, BS,[1] Stephen Dusza, DrPH,[1] Jilliana Monnier, MD,[1,7] Piyush Kumar, PhD,[8] Christi Fox, MS,[9] Christian Brand, PhD,[10] Sheryl Roberts, PhD,[4] Kivanc Kose, PhD,[1] William Phillips, BS,[1] Erica Lee, MD,[1] Chih-Shan Jason Chen, MD, PhD,[1] Anthony Rossi, MD,[1] Kishwer Nehal, MD,[1] Melissa Pulitzer, MD,[1] Caterina Longo, MD,[11,12] Allan Halpern, MD,[1] Thomas Reiner, PhD,[4,13, 14] Milind Rajadhyaksha, PhD,[1*] Manu Jain, MD[1*#]

* senior authors

Running title: PARPi-FL in basal cell cancer diagnosis

[1]Dermatology Service, MSKCC, New York, USA.

[2]University of Puerto Rico - Medical Sciences Campus, San Juan, Puerto Rico.

[3]SUNY Upstate Medical University, Syracuse, USA.

[4]Department of Radiology, MSKCC, New York,

[5]Department of Nuclear Medicine, University Hospital Klinikum Rechts der Isar and Central Institute for Translational Cancer Research (TranslaTUM), Technical University Munich, Munich, Germany

[6]Department of Chemistry, Technical University Munich, Munich, Germany

[7]Dermatology department and Skin cancer department, La Timone Hospital, AP-HM, Aix-Marseille University, Marseille, France

[8]Department of Environmental Medicine and Public Health, Icahn School of Medicine at Mt. Sinai, New York, USA

[9]Caliber Imaging and Diagnostics, Rochester, USA

[10]Summit Biomedical Imaging, New York, USA

[11]Department of Dermatology, University of Modena and Reggio Emilia, Modena, Italy

[12]Azienda Unità Sanitaria Locale – IRCCS di Reggio Emilia, Centro Oncologico ad Alta Tecnologia Diagnostica-Dermatologia, Reggio Emilia, Italy

[13]Department of Radiology, Weill Cornell Medical College, NY, USA

[14]Chemical Biology Program, MSKCC, NY, US

First Author:

Dr. Aditi Sahu, Ph.D. (0000-0003-0004-3839)

Research Associate

530E, 74th street

MSKCC, New York-10021, NY.

Email: sahua@mskcc.org

Phone: 646-608-1935

[#]Corresponding author:

Dr. Manu Jain, MD

Assistant Attending

530E, 74th street

MSKCC, New York-10021, NY.

Email: jainm@mskcc.org

Phone: 646-608-3562

Reprint requests: Manu Jain

Manuscript word count: 4994

=

Keywords: basal cell carcinoma; cancer diagnosis; reflectance confocal microscopy; nuclear contrast; fluorescence confocal microscopy; in vivo

ABSTRACT:

Reflectance confocal microscopy (RCM) with endogenous backscattered contrast can noninvasively image basal cell carcinomas (BCCs) in skin. However, BCCs present with high nuclear density and the relatively weak backscattering from nuclei impose a fundamental limit on contrast, detectability, and diagnostic accuracy. We investigated PARPi-FL, an exogenous nuclear poly (ADP-ribose) polymerase (PARP1)-targeted fluorescent contrast agent and fluorescence confocal microscopy (FCM) towards improving BCC diagnosis.

Methods: We tested PARP1 expression in 95 BCC tissues using immunohistochemistry, followed by PARPi-FL staining in 32 fresh surgical BCC specimens. Diagnostic accuracy of PARPi-FL contrast was evaluated in 83 surgical specimens. Optimal parameters for trans-epidermal permeability of PARPi-FL through intact skin was tested *ex vivo* on 5 human skin specimens and *in vivo* in 3 adult Yorkshire pigs.

Results: We found significantly higher PARP1 expression and PARPi-FL binding in BCCs, as compared to normal skin structures. Blinded reading of RCM-and-FCM images by two experts demonstrated a higher diagnostic accuracy for BCCs with combined fluorescence and reflectance contrast, as compared to RCM-alone. Optimal parameters (time and concentration) for PARPi-FL trans-epidermal permeation through intact skin were successfully determined.

Conclusion: Combined fluorescence and reflectance contrast may improve noninvasive BCC diagnosis with confocal microscopy.

INTRODUCTION

Basal cell carcinomas (BCCs) occur with high incidence rates of more than 4 million in the US, Europe and Australia every year.**(*1*)** Diagnosis is based on dermoscopy followed by biopsy and histopathology. BCC can manifest as superficial, nodular, infiltrative, and micronodular subtypes.**(*2*)** While dermoscopy provides high sensitivity (80-100%), the specificity remains low and variable (32-90%), particularly for lesions lacking distinct pigmentation and/or vascular patterns (so-called "pink lesions")**(*3-5*)**. This lower specificity leads to approximately 3 to 5 benign lesions being biopsied for every detected malignancy, which translates to roughly 12-15 million biopsies annually**(*6*)**. The specificity for BCC diagnosis has been recently improved with reflectance confocal microscopy (RCM).

RCM is a noninvasive high-resolution label-free "quasi-histopathological" imaging technique that shows cellular-level morphology and architecture in skin to a depth of 200 µm**(*7-9*)**. RCM is based on the detection of singly back-scattered light from sub-surface optical sections**(*10-13*)**. RCM detects BCCs with sensitivity of 76-94% and specificity of 54-95%**(*14-16*)**. When combined with dermoscopy, RCM provides ~50% higher specificity, with a resulting ~2x drop in the benign-to-malignant biopsy ratio compared to dermoscopy-alone**(*17-19*)**. Although the use of RCM has improved diagnostic accuracy at-the-bedside, the backscattered contrast imposes a *fundamental limit* for BCC diagnosis. Due to weak backscatter from intra-nuclear chromatin, nuclear-dense BCCs appear dark relative to the surrounding dermis. But nuclear-dense normal structures (hair follicles, lower basal cell layer of epidermis) also appear dark, thus mimicking BCCs**(*16,20*)**. This limitation may be overcome with an exogenous molecular-targeted fluorescence nuclear contrast agent and fluorescence confocal microscopy (FCM) imaging.

PARPi-FL is a newly developed small-molecule (620 Da), poly (ADP-ribose) polymerase (PARP1)-targeted fluorescent reporter**(*21*)**. PARPi-FL is BODIPY-FL conjugated to PARP inhibitor Olaparib , possessing strong PARP1 specificity of Olaparib **(*22,23*)** and strong fluorescence properties of BODIPY-FL, and has shown specific nuclear labeling and tumor imaging **(*24,25*)**. The federal drug administration accorded investigational new drug status to PARPi-FL, and a Phase I/II trial is in progress (NCT03085147)

for imaging oral cancers in patients**(*26,27*)**. Higher intra-nuclear accumulation in tumors, rapid tissue permeation [4.6 μm/s**(*28*)**], safety, and detectability deeper in tissue makes PARPi-FL attractive for BCC diagnosis.

However, for *in vivo* use in patients, two central questions must be addressed: 1) Can the exogenous PARPi-FL nuclear contrast improve the diagnostic accuracy for BCCs? 2) Can PARPi-FL be quickly and effectively delivered trans-epidermally to BCCs in the dermis through intact skin? We report the results of our investigation on PARP1 expression, PARPi-FL staining, and permeability in this article**(Figure 1)**.

METHODS

Sample Collection

PARP1 expression was investigated on formalin-fixed-paraffin-embedded (FFPE) specimens. For experiments on PARPi-FL staining, surgically excised *fresh* discarded BCC and normal specimens were collected after Mohs surgeries. For the permeability experiments, large (5 cm x 5 cm) specimens of normal breast skin were collected at the end of mastectomies. All samples were collected under various IRB-approved protocols.

PARP1 Expression in BCCs

Two adjacent thin (5 μm) FFPE sections were obtained for PARP1 immunohistochemistry (IHC) and Hematoxylin & Eosin (H&E). PARP1-IHC was performed according to previously described procedure **(*24*)**. We used an anti-PARP1 rabbit monoclonal antibody (46D11, Cell Signaling Technology, Danvers, MA) at 0.4 μg/mL, followed by a biotinylated goat anti-rabbit IgG (PK6106, Vector Labs, Burlingame, CA) at a 1:200 dilution.

Quantification of PARP1 Expression

IHC-stained and H&E-stained sections were digitally scanned (Aperio ScanScope Slide Scanner, Leica Biosystems, IL, US). BCCs and surrounding normal structures - hair follicles, sebaceous glands, and epidermis - were annotated by a pathologist (MJ) using different color codes. PARP1 was quantified using Positive Pixel counting algorithm (Aperio, Leica Biosystems, IL, US)(*29*). Thresholding was performed on

diaminobenzidine PARP1 positive area and total area was determined by hematoxylin-stained area. PARP1-positivity (integrated positive pixel area/total annotated area) was computed in each field-of-view (FOV). Thresholds, hue, and saturation were kept constant for all specimens.

PARPi-FL Staining and Nuclear PARP1 Specificity in Thin Tissue Sections

Fresh discarded BCC tissues were serial sectioned into four 10 µm frozen sections for PARPi-FL, H&E, PARP1 immunofluorescence (IF) test, and isotype IgG control **(Supplemental Figure 1A).** For PARPi-FL staining, tissue sections were stained with 100 nM PARPi-FL (in 30% polyethylene glycol, PEG) for 5 minutes using Hoechst 33342 (Invitrogen, Carlsbad, CA, US) 0.002 mg/mL as a nuclear counterstain. IF was performed using a previously described procedure **(*24*).** We used anti-PARP1 Ab (rabbit polyclonal IgG, SC-7150, Santacruz Biotechnology, 1: 200 dilution) and isotype control (normal rabbit IgG, Santacruz Biotechnology, 1:200 dilution), and AlexaFluor 568 goat-anti-rabbit, A21076, Molecular probes, Invitrogen, 1:1000 dilution as the secondary Ab. The slides were scanned using a Mirax Slide Scanner (3DHISTECH, Budapest, Hungary). For selected tissues, 10-15 PARPi-FL images were also acquired with a commercial microscope (LSM880, Carl Ziess Microscopy LLC, Germany) in tumor and normal areas. Analysis for fluorescence intensity and area positivity on the microscopic images was performed using a batch-code implemented in FIJI. Thresholding was performed for PARPi-FL signal, and total nuclear area was calculated using Hoechst to calculate normalized intensity and area positivity. Analysis was done on image-level and case-level (average of multiple images).

PARPi-FL Staining in Thick fresh BCC specimens

Specimens were stained with PARPi-FL (250 nM PARPi-FL in 30% PEG300/PBS for 10 min, followed by 10 min in 30% PEG300/PBS) and imaged using a benchtop research *ex vivo* RCM-and-FCM prototype microscope (Vivascope-2500; Caliber Imaging and Diagnostics, Rochester, US) simultaneously in both fluorescence (488 nm) and reflectance (785 nm) modes **(Supplemental Figure 1B)**. RCM and FCM mosaicking to display up to 12 mm x 12 mm FOV encompassing the entire tissue was performed and used for the blinded study.

Blinded Reader Evaluation

The blinded reading study was performed by two expert confocal readers (MJ, CL). Training was on a subset of RCM and FCM mosaics with equal number of BCC positive and negative cases (i. e., equal prevalence for BCCs and normal skin). Depending on the specimen size , each mosaic was divided in either 2 or 4 sub-mosaics to facilitate reading. The diagnosis was evaluated at both mosaic (case-level) and individual sub-mosaic (quadrant-level). Both readers were provided with matched RCM and FCM mosaics for each specimen. RCM mosaic was evaluated, followed by matched FCM mosaic to compare BCC diagnostic accuracy on RCM, and with added PARPi-FL contrast in RCM+FCM . Readers evaluated BCC presence/absence, nuclear staining (on FCM), and overall diagnostic quality. Blinded analysis results were compared with the corresponding H&E to compute sensitivity, specificity, positive, and negative predictive values at case-level and quadrant-level.

Effect of PARPi-FL on Subsequent Histopathology

Normal and BCC tissues were bisected such that one piece was immersed in PARPi-FL (1 µM) and other in PEG-PBS (control) for 30 minutes, respectively. Both pieces were separately submitted in formalin for H&E-histopathology evaluation. Sections were digitally scanned and blindly read by two pathologists (MJ, MP) to grade: a) staining quality of cytoplasm, nucleus, and collagen, b) diagnostic acceptability or unacceptability, and c) BCC presence/absence and subtype.

Permeability and Trans-epidermal Delivery in *ex vivo* Tissue

The mastectomy specimens were processed to remove adipose tissue and blood without disrupting stratum corneum integrity. Tissues were placed on a flat corkboard and gently wiped with an alcohol pad (Webcol alcohol preps, Covidien, Walpole, MA) and allowed to dry. PARPi-FL was applied topically on the stratum corneum using plastic and metal templates, which served as PARPi-FL reservoirs **(Supplemental Figure 1C)**. Additionally, in some specimens, a PARPi-FL saturated gauze (1 µM) followed by Tegaderm® patch (3M Medical, St. Paul, MN, US) was pinned on the skin to maintain uniform pressure, to mimic topical application and occlusion *in vivo*. A range of PARPi-FL concentrations (1-10

μM) and application times (10-30 minutes) were tested. After experiment completion, a 5-mm punch biopsy (MediChoice® biopsy punches, Owens and Minor, Richmond, VA, US) was performed. Each biopsy was bisected and dipped in Hoechst 33342 (Invitrogen, Carlsbad, CA, US) (diluted to 1 μL/ml in chilled PBS) for nuclear counterstaining. The tissues were mounted on their lateral surface for imaging with a confocal microscope (Zeiss LSM880 system (20x/0.8 NA) using 405 nm (Hoechst) and 488 nm (PARPi-FL) wavelengths. The raw files were qualitatively visualized in FIJI.

Permeability and Trans-epidermal Delivery *in vivo*

Topical application and permeability were tested *in vivo* in adult female Yorkshire pigs obtained under an approved IACUC protocol. The pigs were anesthetized using inhalational 5% isoflurane. A ~18 inches across area on the flank was selected, shaved and gently swabbed with ethanol. Any local irritation (confirmed visually) from shaving was allowed to subside before PARPi-FL application. Within this area, two sets of rows comprising five sites each were marked for the well placement to deliver either PARPi-FL or saline and to perform biopsies **(Supplemental Figure 1D)**. Each application site was spaced 2 cm apart (edge-to-edge) to prevent cross contamination. Each well (or template) (Everbilt, Home Depot Product Authority, LLC) measured 3/8-inch in diameter and was attached to the selected site using an adhesive (Dermabond Advanced®; Ethicon US, LLC) in which 1 mL of 10 μM PARPi-FL or saline solution was left for 30 minutes. Subsequently, ten 8-mm punch biopsies were performed on each pig. The biopsies were bisected, one piece was submitted for H&E-staining and the other was promptly imaged using the benchtop *ex vivo* RCM-and-FCM microscope (Vivascope-2500; Caliber ID). The biopsies were processed for histopathology.

Statistical Analysis

Analyses were conducted using GraphPad Prism 8.0, Stata (v 14.2; Stata Corp, College Station, TX), and R (R Core Team, 2020) with packages “rel” (LoMartire, 2020) to calculate agreement statistics and “ggplot2” (Wickham, 2016) to produce figures. Inferential unpaired sample comparisons were assessed by the Mann-Whitney U test. PARPi-FL intensity and area positivity were converted by natural log

transform because the raw data was right skewed. Associations of transformed variables with clinical outcomes were analyzed with receiver operating characteristic (ROC) curves. A blinded experiment was conducted to assess diagnostic accuracy on RCM and RCM+FCM of two expert readers. Interrater agreement on the presence of cellular level features, diagnosis subtyping, and binarized tissue quality assessments were quantified according to Gwet's AC1 due to high marginal imbalance in the sample in addition to overall percent agreement. For the effect of PARPi-FL on histopathology, agreement between pathologists was quantified according to Gwet's AC1. Statistical significance was determined with $\alpha = 0.05$. Unless stated otherwise, data are presented as mean ± s.d and significance are specified ($^{*}p < 0.05$, $^{**}p < 0.01$, $^{***}p < 0.001$, $^{****}p < 0.0001$).

RESULTS

PARP1 Expression in BCC and Normal Skin Structures

In 95 specimens, we found PARP1 expression in BCCs (subtypes - superficial, nodular, infiltrative and micronodular) and in normal structures **(Figure 2A, Supplemental Figure 2)**. Higher area positivity was observed in tumors (47.89% ± 21.4), followed by hair follicles, epidermis, and sebaceous glands *($p < 0.001$)* **(Figure 2B)**. Area under the curve (AUC) value of 0.927 indicates successful discrimination of tumor and normal areas based on PARP1 area positivity **(Figure 2C)**.

PARPi-FL Staining and PARP1-immunofluorescence in BCC Thin sections

In 32 thin BCC sections, PARPi-FL uptake in nuclei correlated with PARP1 expression, confirmed by PARP1-IF **(Figure 3A, B and Supplemental Figure 3A, B)**. The fluorescence intensity and area positivity in 394 images (from 32 tissues) demonstrated significantly higher intensity and area positivity in tumors relative to that in normal tissue ($p<0.01$) with both image-wise and case-wise analysis **(Figure 3C, Supplemental Figure 3C).** Similar trends were observed in non-transformed data **(Supplemental Figure S3D, E).** Area positivity differentiated tumor and normal with high accuracy (AUC 0.96) than fluorescence intensity (AUC 0.68) **(Figure 3D)**.

PARPi-FL Staining for Improving BCC Diagnosis in an *ex vivo* Blinded Study

In 83 fresh surgical specimens, PARPi-FL enhanced the visualization of small BCC tumors that otherwise were invisible in the corresponding RCM mosaic, as confirmed on H&E **(Figure 4A, Supplemental Figure 4)**. Of the 166 RCM and FCM mosaics, 44 were used for training. Blinded evaluation was performed on the remaining 122 mosaics, however only cases with acceptable diagnostic quality were analyzed. We found higher sensitivity and moderate increase in specificity in the RCM+FCM images as compared to RCM-alone **(Figure 4B, C).**

Transepidermal Delivery of PARPi-FL Through Intact Skin in Fresh *ex vivo* Human Specimens

In five *ex vivo* normal mastectomy specimens, we tested topical application of PARPi-FL at various concentrations and application times **(Figure 5)**.We detected PARPi-FL staining in the nuclei of basal cells of epidermis and dermal cells, confirming successful permeability. Optimal staining with high nuclear specificity and intensity was observed for 10 μM PARPi-FL concentration when applied for 30 minutes. These parameters were selected for *in vivo* testing in pigs.

Transepidermal Delivery of PARPi-FL in a *in vivo* Pig Model

In three adult Yorkshire pigs, we verified PARPi-FL permeability *in vivo* in normal skin following topical application of 10 μM PARPi-FL for 30 minutes **(Figure 6, Supplemental Figure 5)**. Positive nuclear staining in the epidermal basal cell layer was consistently observed in PARPi-FL treated sites, and was absent in the control sites, confirming the permeability and detectability of PARPi-FL after *in vivo* application. No significant histopathological differences were noticeable between the PARPi-FL treated and control groups **(Figure 6, Supplemental Figure 6).**

DISCUSSION

Our results suggest that the addition of exogenous PARPi-FL fluorescence contrast to endogenous reflectance contrast may improve non-invasive diagnosis of BCC. PARP1 proved to be an excellent biomarker; we found consistently higher PARP1 expression in all BCC subtypes, as compared to normal skin structures. Across the 95 specimens investigated, 90% BCCs had homogenous PARP1 staining,

especially in superficial and infiltrative subtypes. Some heterogenous PARP1 expression was observed in a few nodular BCCs (<10%), specifically in the variants with nodular-cystic changes and squamous differentiation (**Supplemental Figure 2E)**.

We confirmed specific nuclear labeling correlating with PARP1 expression in nucleated tissue areas of tumors, basal epidermal layers in epidermis, hair follicles and sebaceous glands **(Figure 3A, B Supplemental Figure 3A, B)**. **We used area positivity and intensity parameters to quantitatively confirm PARPi-FL nuclear fluorescence in tumors as compared to normal nucleated structures that often confounds BCC diagnosis *in vivo*. Although both parameters were** higher in tumors, only area positivity could successfully differentiate tumor from normal with a high accuracy **(Figure 3D)**. **We acknowledge that none of these parameters would have utility in clinical practice (as Hoechst or other nuclear dye cannot be applied on patients); however, PARPi-FL staining would enhance the cellular and morphological details that would aid an expert RCM reader to differentiate BCC from normal structures and improve the diagnosis.** This was also demonstrated through the blinded analysis performed by 2 expert RCM readers, where PARPi-FL contrast when combined with RCM boosted the diagnostic accuracy, as compared to RCM-alone. In general, nuclear staining was observed in most tissues, only 5/62 (8%) tissues had minimal or no nuclear staining in tumor and/or normal structures. This was in contrast to the PARP1 expression, where only 1.1% specimens showed low or negative expression. A higher rate of inconsistent nuclear staining could be attributed to the delays in fresh tissue handling since PARP1 can rapidly degrade in excised tissues. Despite, some heterogeneity in PARPi-FL nuclear labeling, we demonstrated that a combined imaging approach (RCM+FCM) improved diagnostic performance, especially sensitivity, when compared to RCM-alone. Surprisingly, we **found minimal improvements in specificity in the blinded study. False positives were more prevalent in cases with "smudged" PARPi-FL staining, possibly attributed to the variability in tissue quality. Furthermore, *ex vivo* tissues, do not image as well as skin *in vivo, (30-32),* probably due to tissue dehydration and alteration in refractive index and optical properties. Differences in the training of the two readers could also**

impact differential improvements in sensitivity and specificity. We do not anticipate these tissue-related issues during *in vivo* imaging in patients (our ultimate goal). Thus, we expect better results, in terms of both higher sensitivity and specificity, with use of RCM+FCM imaging, when performed in patients through a clinical trial.

Next critical issue that makes a contrast agent suitable for topical application is permeability through intact skin. We successfully demonstrated that PARPi-FL can passively diffuse through the stratum corneum after topical application in *ex vivo* human tissues and in *in vivo* pig skin. Skin is characterized by a tightly and coordinately regulated molecular transport system, which allows molecules with low molecular weight (<500 Da) and lipophilicity (logP: 1-3) to permeate the stratum corneum. Thus, the borderline molecular weight and lipophilicity of PARPi-FL (620 Da, logP:2.9) makes it suitable for topical application and trans-epidermal delivery. We found that PARPi-FL at 10 µM concentration and 30 minutes yielded consistent labeling in nucleated cells throughout the epidermis into the dermis in human and pig tissues. To deliver the dye, we attached reservoirs to the skin; however this delivery approach would not be feasible in patients. Thus, to demonstrate clinical feasibility, we also tested PARPi-FL permeability and detectability using a saturated gauze (mimicking a nicotine patch) applied to the skin under occlusion, which yielded similar results **(Supplemental Figure 5)**, laying the foundation for developing a cream or gel-based formulation for topical application in clinics. Furthermore, PARPi-FL application to skin did not influence the subsequent H&E-staining of tissue **(Supplemental Figure 6)**.

CONCLUSION

Higher PARP1 expression was found in BCC as compared to normal skin structures, which would allow specific PARPi-FL labeling in BCCs. Enhanced contrast provided by PARPi-FL labelled nuclei leads to higher sensitivity and specificity for BCC diagnosis with RCM+FCM imaging, compared to RCM-alone. PARPi-FL can be delivered into the dermis (1-10 µM, 10-30 minutes), following passive topical application, suggesting promising potential for clinical use in patients. However, staining was found to be

heterogenous in 8% of thick specimens, suggesting that a combination of FCM with RCM may be necessary for improving clinical diagnosis of BCCs *in vivo* in patients.

ACKNOWLEDGEMENTS

We acknowledge Dr. Evan Matros and the PPBC team, Mr. Brandon Possum and Mohs Lab, Eric Chan and MCCF Core, MSK-Animal Imaging Core Facility, the Radiochemistry & Molecular Imaging Probes Core, the Nuclear Magnetic Analytical Core, and the MSK Center for Molecular Imaging & Nanotechnology. This work was supported by National Institutes of Health grants P30 CA008748, R01 EB020029 (MR) and R01 CA204441 (TR), the MSK Imaging and Radiation Sciences Program and the MSK Society Grant (MJ). The funding sources were not involved in study design, data collection and analysis, writing of the report, or the decision to submit this article for publication.

CONFLICTS OF INTEREST

T.R., S.K. and C.B. are shareholders of Summit Biomedical Imaging, LLC. T.R. and S.K. are co-inventors on filed U.S. patent (WO2016164771) held by MSK that covers methods for PARPi-FL. T.R. is a co-inventor on U.S. patent (WO2012074840) held by the General Hospital Corporation that covers PARPi-FL composition. T.R. is a paid consultant for Theragnostics, Inc. C.B. serves as Chief Scientific Officer at Summit Biomedical Imaging, LLC. Christi Alessi-Fox is a former employee, holds equity in and currently a consultant with Caliber Imaging and Diagnostics. Milind Rajadhyaksha is a former employee of and owns equity in Caliber Imaging and Diagnostics. The VivaScope is the commercial version of an original laboratory prototype that he developed at Massachusetts General Hospital, Harvard Medical School. No other potential conflicts of interest relevant to this article exist.

KEY POINTS

Question: Can PARPi-FL combined with reflectance contrast improve detection of basal cell carcinoma (BCC)?

Pertinent findings: Higher PARP1 expression and PARPi-FL staining confirmed in nuclei of tumor cells as compared to normal skin structures. In a blinded study by two readers, diagnostic accuracy for BCCs was higher for combined PARPi-FL and reflectance contrast as compared to reflectance contrast alone. The permeability of PARPi-FL through passive diffusion was also confirmed in human skin and in vivo in pigs.

Implications for patient care: Improving non-invasive diagnosis will directly impact clinical care and management of BCC by reducing benign biopsies and enabling non-surgical management of less-aggressive BCC subtypes.

REFERENCES

1. Rogers HW, Weinstock MA, Feldman SR, Coldiron BM. Incidence Estimate of Nonmelanoma Skin Cancer (Keratinocyte Carcinomas) in the U.S. Population, 2012. *JAMA Dermatol.* 2015;151:1081-1086.

2. Bichakjian C, Armstrong A, Baum C, et al. Guidelines of care for the management of basal cell carcinoma. *J Am Acad Dermatol.* 2018;78:540-559.

3. Wozniak-Rito A, Zalaudek I, Rudnicka L. Dermoscopy of basal cell carcinoma. *Clinical and experimental dermatology.* 2018;43:241-247.

4. Reiter O, Mimouni I, Gdalevich M, et al. The diagnostic accuracy of dermoscopy for basal cell carcinoma: a systematic review and meta-analysis. *J Am Acad Dermatol.* 2019;80:1380-1388.

5. Altamura D, Menzies SW, Argenziano G, et al. Dermatoscopy of basal cell carcinoma: morphologic variability of global and local features and accuracy of diagnosis. *J Am Acad Dermatol.* 2010;62:67-75.

6. Dinnes J, Deeks JJ, Chuchu N, et al. Visual inspection and dermoscopy, alone or in combination, for diagnosing keratinocyte skin cancers in adults. *Cochrane Database of Systematic Reviews.* 2018.

7. Rajadhyaksha M, Grossman M, Esterowitz D, Webb RH, Anderson RR. In vivo confocal scanning laser microscopy of human skin: melanin provides strong contrast. *J Invest Dermatol.* 1995;104:946-952.

8. Rajadhyaksha M, González S, Zavislan JM, Anderson RR, Webb RH. In vivo confocal scanning laser microscopy of human skin II: advances in instrumentation and comparison with histology. *J Invest Dermatol.* 1999;113:293-303.

9. Rajadhyaksha M, Anderson RR, Webb RH. Video-rate confocal scanning laser microscope for imaging human tissues in vivo. *Appl Opt.* 1999;38:2105-2115.

10. Guitera P, Menzies S, Argenziano G, et al. Dermoscopy and in vivo confocal microscopy are complementary techniques for diagnosis of difficult amelanotic and light-coloured skin lesions. *Br J Dermatol.* 2016;175:1311-1319.

11. Ruini C, Hartmann D, Saral S, Krammer S, Ruzicka T, von Braunmühl T. The invisible basal cell carcinoma: how reflectance confocal microscopy improves the diagnostic accuracy of clinically unclear facial macules and papules. *Lasers Med Sci.* 2016;31:1727-1732.

12. Nelson SA, Scope A, Rishpon A, et al. Accuracy and confidence in the clinical diagnosis of basal cell cancer using dermoscopy and reflex confocal microscopy. *Int J Dermatol.* 2016;55:1351-1356.

13. Liopyris K, Navarrete-Dechent C, Yélamos O, Marchetti M, Rabinovitz H, Marghoob A. Clinical, dermoscopic and reflectance confocal microscopy characterization of facial basal cell carcinomas presenting as small white lesions on sun-damaged skin. *The British journal of dermatology.* 2019;180:229.

14. Dinnes J, Deeks JJ, Saleh D, et al. Reflectance confocal microscopy for diagnosing cutaneous melanoma in adults. *Cochrane Database of Systematic Reviews.* 2018.

15. Lupu M, Popa IM, Voiculescu VM, et al. A Retrospective Study of the Diagnostic Accuracy of In Vivo Reflectance Confocal Microscopy for Basal Cell Carcinoma Diagnosis and Subtyping. *J Clin Med.* 2019;8.

16. Jain M, Pulijal SV, Rajadhyaksha M, Halpern AC, Gonzalez S. Evaluation of Bedside Diagnostic Accuracy, Learning Curve, and Challenges for a Novice Reflectance Confocal Microscopy Reader for Skin Cancer Detection In Vivo. JAMA Dermatol. 2018;154(8):962-965. doi:10.1001/jamadermatol.2018.1668.

17. Witkowski A, Łudzik J, DeCarvalho N, et al. Non-invasive diagnosis of pink basal cell carcinoma: how much can we rely on dermoscopy and reflectance confocal microscopy? *Skin Res Technol.* 2016;22:230-237.

18. Xiong Y-Q, Ma S-J, Mo Y, Huo S-T, Wen Y-Q, Chen Q. Comparison of dermoscopy and reflectance confocal microscopy for the diagnosis of malignant skin tumours: a meta-analysis. *Journal of Cancer Research and Clinical Oncology.* 2017;143:1627-1635.

19. Witkowski A, Łudzik J, Arginelli F, et al. Improving diagnostic sensitivity of combined dermoscopy and reflectance confocal microscopy imaging through double reader concordance evaluation in telemedicine settings: A retrospective study of 1000 equivocal cases. *PLoS One.* 2017;12:e0187748.

20. Rajadhyaksha MM, Gonzalez S, Zavislan JM. Detectability of contrast agents for confocal reflectance imaging of skin and microcirculation. *Journal of biomedical optics.* 2004;9:323-332.

21. Reiner T, Lacy J, Keliher EJ, et al. Imaging therapeutic PARP inhibition in vivo through bioorthogonally developed companion imaging agents. *Neoplasia.* 2012;14:169IN161-177IN163.

22. Carney B, Kossatz S, Lok BH, et al. Target engagement imaging of PARP inhibitors in small-cell lung cancer. *Nature Communications.* 2018;9:176.

23. Reiner T, Lacy J, Keliher EJ, et al. Imaging therapeutic PARP inhibition in vivo through bioorthogonally developed companion imaging agents. *Neoplasia.* 2012;14:169-IN163.

24. Kossatz S, Brand C, Gutiontov S, et al. Detection and delineation of oral cancer with a PARP1 targeted optical imaging agent. *Sci Rep.* 2016;6:21371.

25. Irwin CP, Portorreal Y, Brand C, et al. PARPi-FL-a fluorescent PARP1 inhibitor for glioblastoma imaging. *Neoplasia.* 2014;16:432-440.

26. Kossatz S, Pirovano G, França PDDS, et al. Validation of the use of a fluorescent PARP1 inhibitor for the detection of oral, oropharyngeal and oesophageal epithelial cancers. *Nature Biomedical Engineering.* 2020;4:272-285.

27. de Souza França PD, Kossatz S, Brand C, et al. A Phase I Study of a PARP1-targeted Topical Fluorophore for the Detection of Oral Cancer. *medRxiv.* 2020:2020.2011.2009.20228536.

28. Thurber GM, Yang KS, Reiner T, et al. Single-cell and subcellular pharmacokinetic imaging allows insight into drug action in vivo. *Nature Communications.* 2013;4:1504.

29. Olson AH. Image analysis using the Aperio ScanScope. *Technical manual Aperio Technologies Inc.* 2006.

30. Rajadhyaksha M, Menaker G, Flotte T, Dwyer PJ, González S. Confocal Examination of Nonmelanoma Cancers in Thick Skin Excisions to Potentially Guide Mohs Micrographic Surgery Without Frozen Histopathology. *J Invest Dermatol.* 2001;117:1137-1143.

31. Patel YG, Nehal KS, Aranda I, Li Y, Halpern AC, Rajadhyaksha M. Confocal reflectance mosaicing of basal cell carcinomas in Mohs surgical skin excisions. *Journal of biomedical optics.* 2007;12:034027.

32. Gareau D, Patel Y, Li Y, et al. Confocal mosaicing microscopy in skin excisions: a demonstration of rapid surgical pathology. *J Microsc.* 2009;233:149-159.

FIGURES:

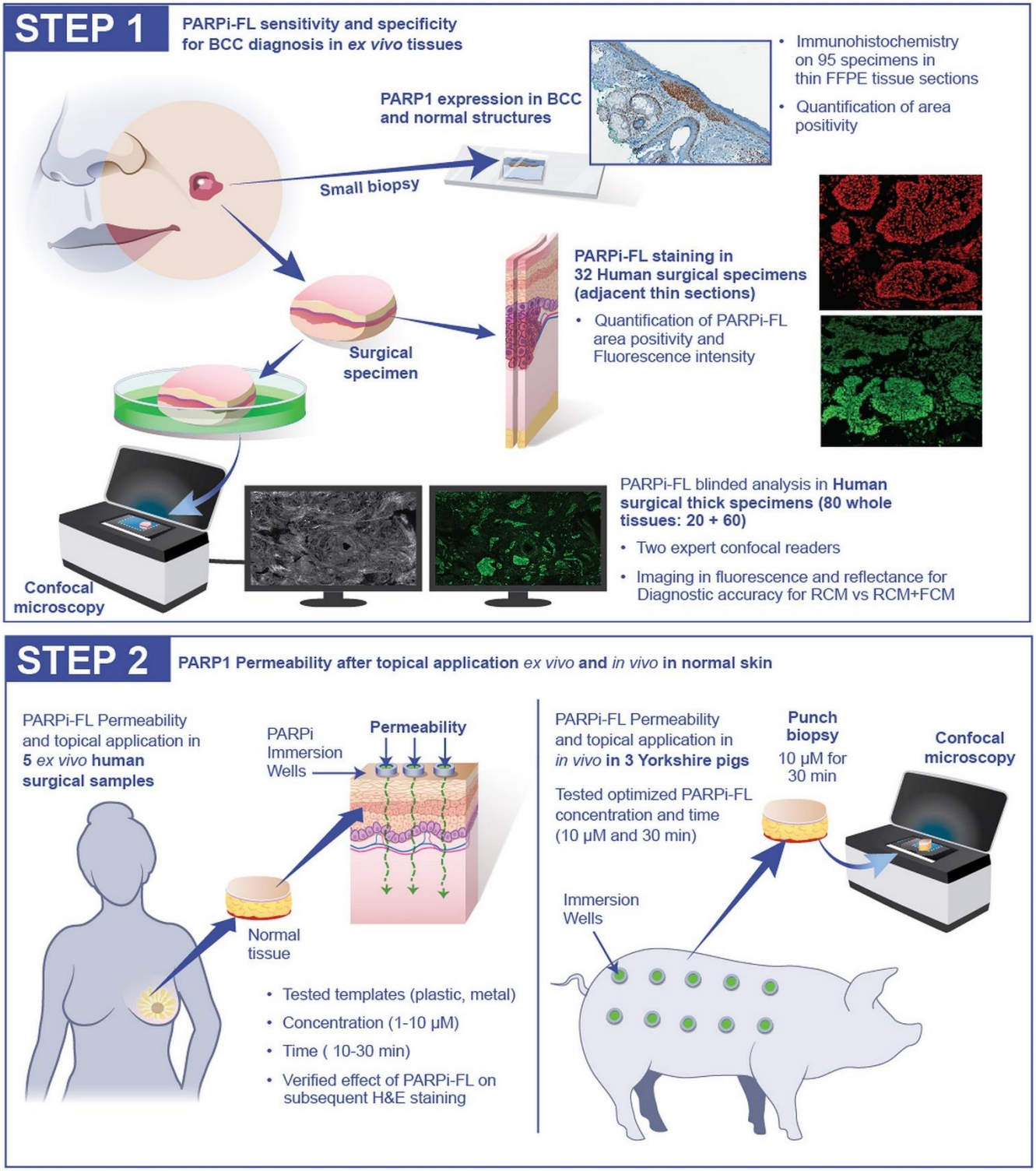

Figure 1. Summary of the experiments undertaken in the study.

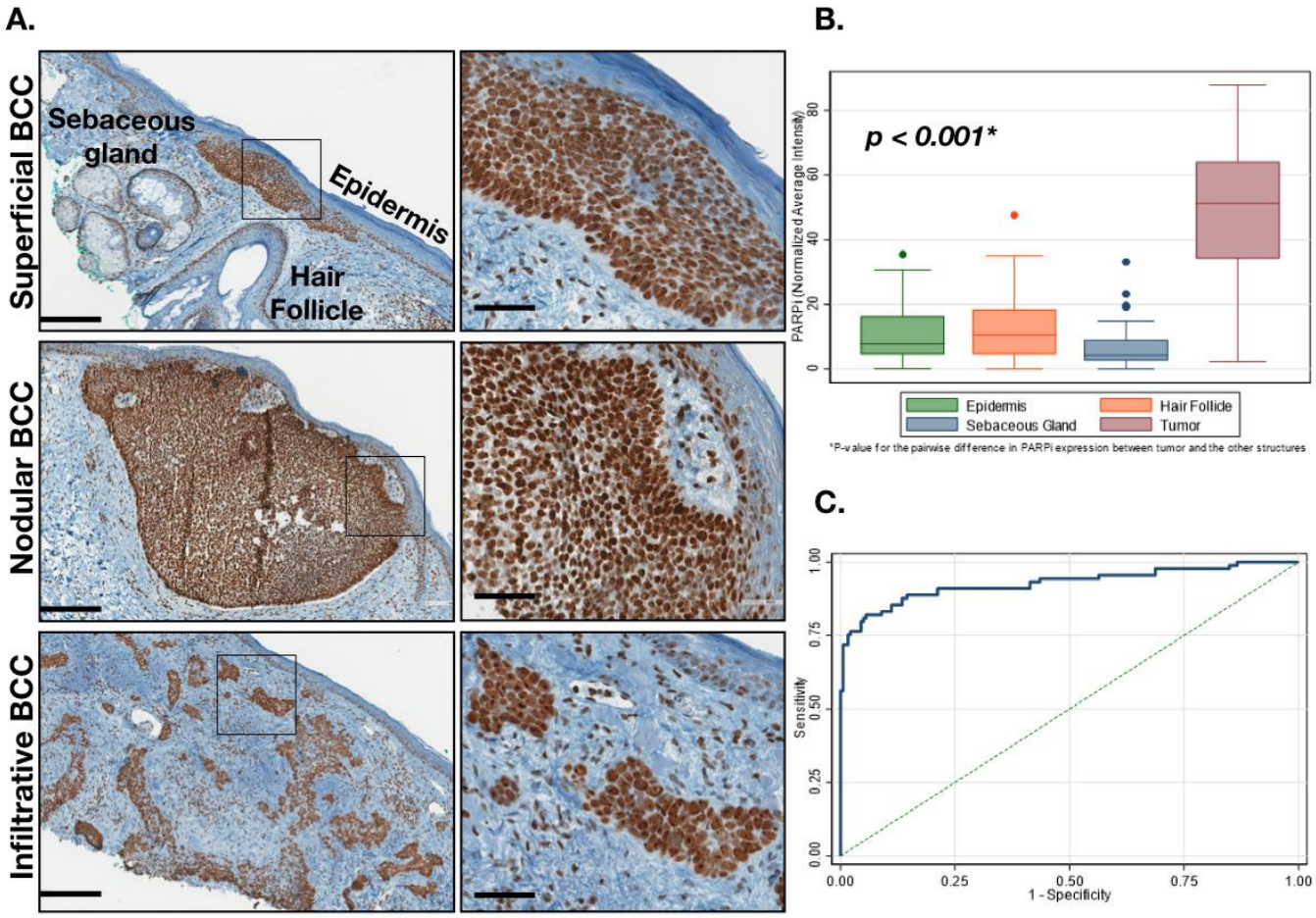

Figure 2. BCCs have higher expression of PARP1 as compared to normal skin structures

A. Representative images of PARP1 expression shows high expression in superficial, nodular and infiltrative BCC, as compared to epidermis, hair follicles, and sebaceous glands; B. PARP1 area positivity in IHC samples (n=95) shows significantly higher positivity in tumors; C. Receiver operating curve to differentiate tumor and normal yields an area-under-the-curve (AUC) of 0.83.

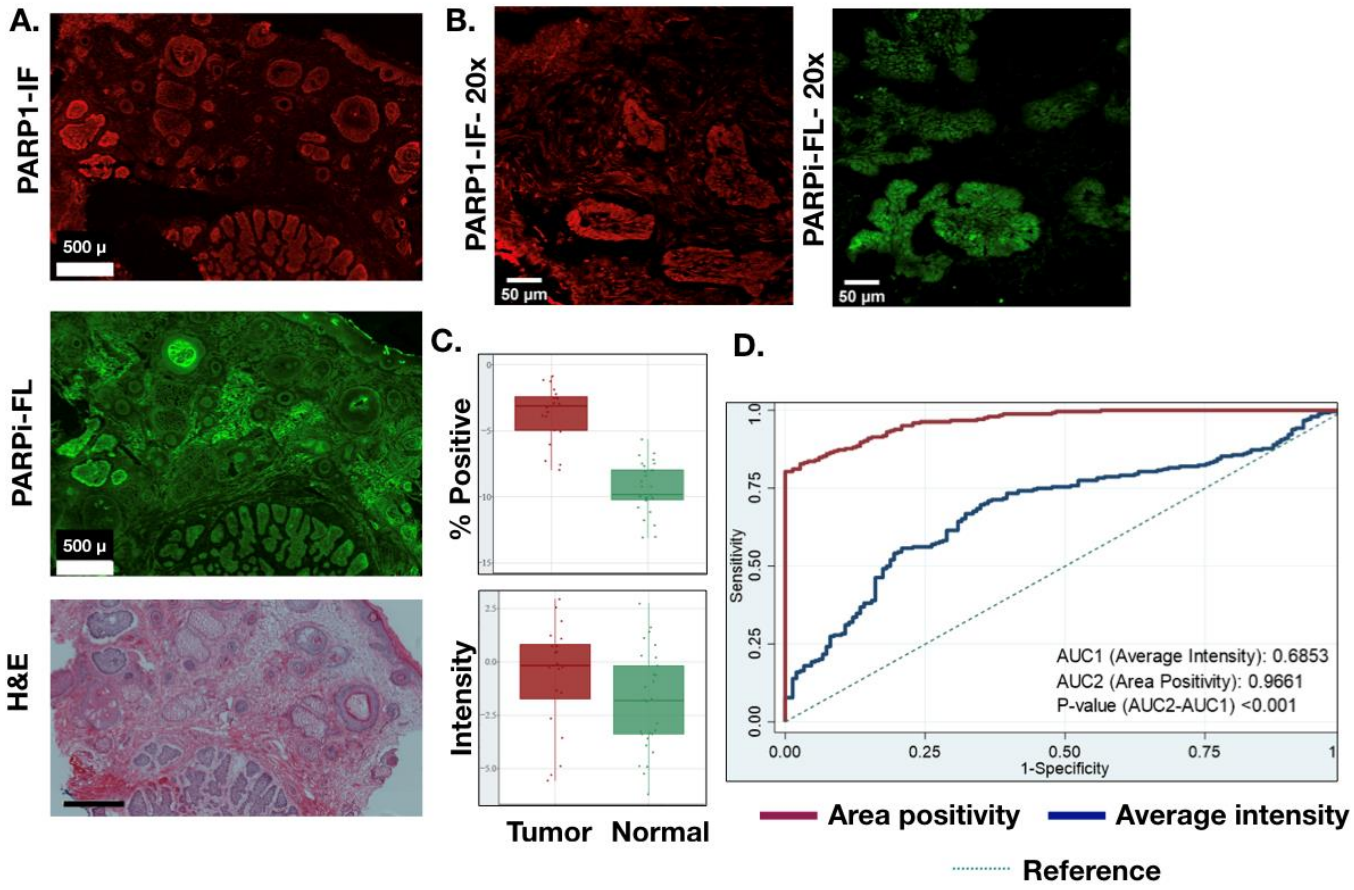

Figure 3. Nuclear specific PARPi-FL staining observed in BCC tissues

A. Representative images showing successful PARPi-FL nuclear staining in tumor and normal. B. PARPi-FL nuclear uptake and spatial correlation with nuclear PARP1 in nucleated areas verified in high-resolution images (Magnification: 20x). C. Higher average intensity and area positivity in tumors as compared to normal structures in case-wise analysis (right) ($p < 0.001$ for % area positivity and image-wise intensity). D. Area positivity shows better discrimination of tumor and normal than fluorescence intensity (AUC 0.96 versus AUC 0.68)

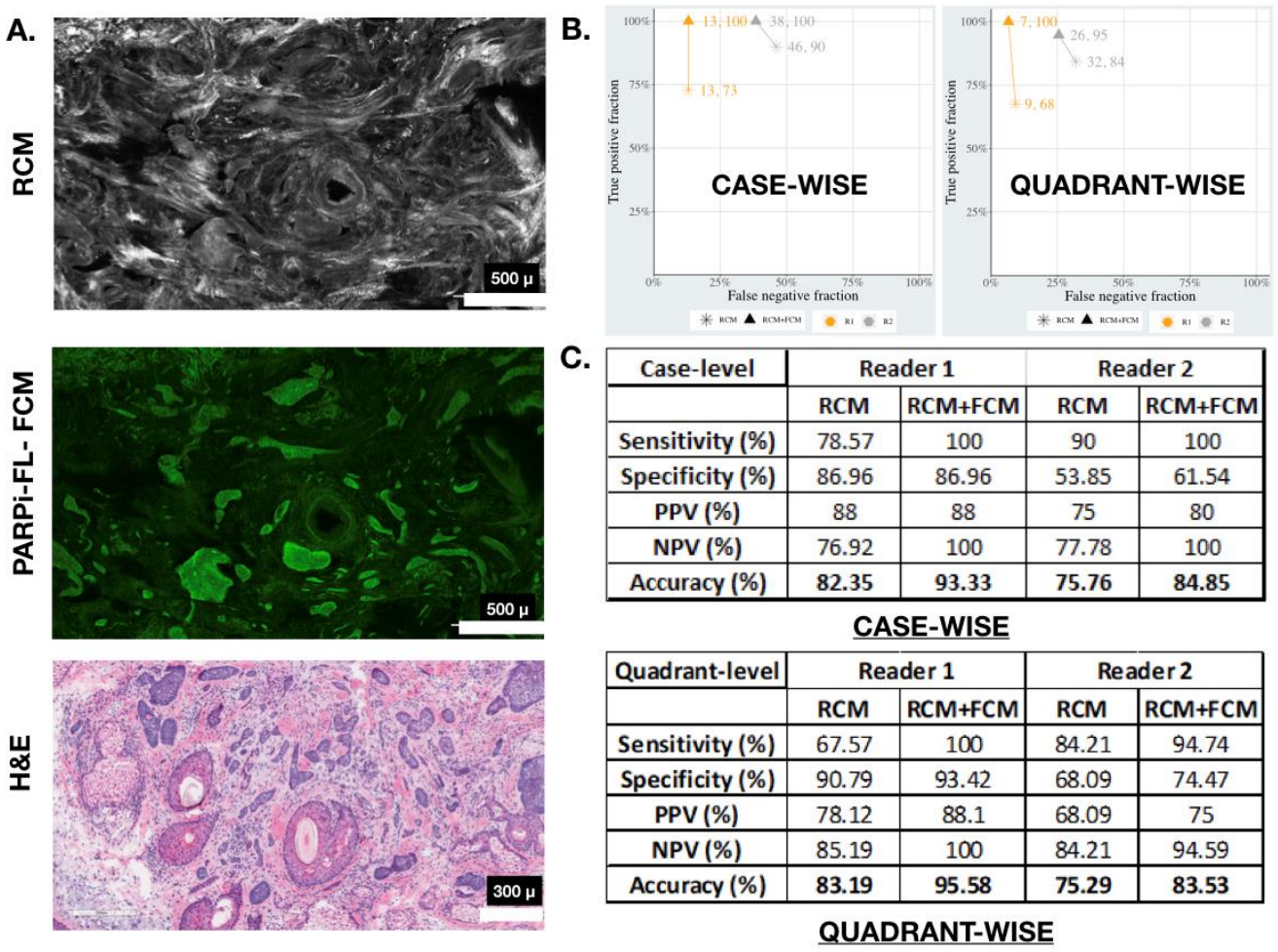

Case-level	Reader 1		Reader 2	
	RCM	RCM+FCM	RCM	RCM+FCM
Sensitivity (%)	78.57	100	90	100
Specificity (%)	86.96	86.96	53.85	61.54
PPV (%)	88	88	75	80
NPV (%)	76.92	100	77.78	100
Accuracy (%)	**82.35**	**93.33**	**75.76**	**84.85**

CASE-WISE

Quadrant-level	Reader 1		Reader 2	
	RCM	RCM+FCM	RCM	RCM+FCM
Sensitivity (%)	67.57	100	84.21	94.74
Specificity (%)	90.79	93.42	68.09	74.47
PPV (%)	78.12	88.1	68.09	75
NPV (%)	85.19	100	84.21	94.59
Accuracy (%)	**83.19**	**95.58**	**75.29**	**83.53**

QUADRANT-WISE

Figure 4. PARPi-FL contrast in FCM images improves BCC diagnostic accuracy over RCM alone

A. PARPi-FL contrast improves visualization of BCCs, as compared to RCM-alone as confirmed on H&E images. B, C. Higher sensitivity in RCM+FCM and moderate increase in specificity found in the blinded evaluation in both case-wise and quadrant-wise analysis.

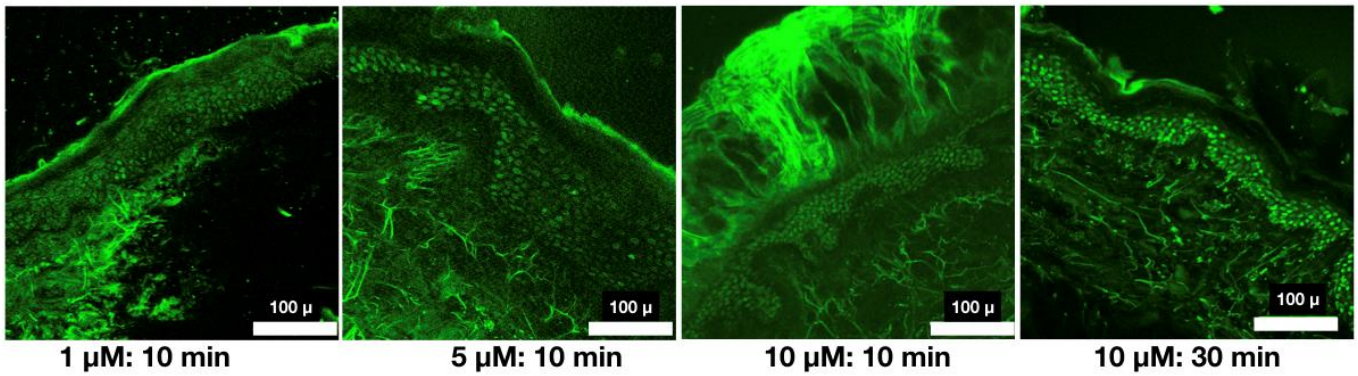

Figure 5. PARPi-FL successfully permeates through intact skin in *ex vivo* human tissue

Increased nuclear labeling found for longer time periods; maximum labeling and intensity found in 10 µM and 30 min.

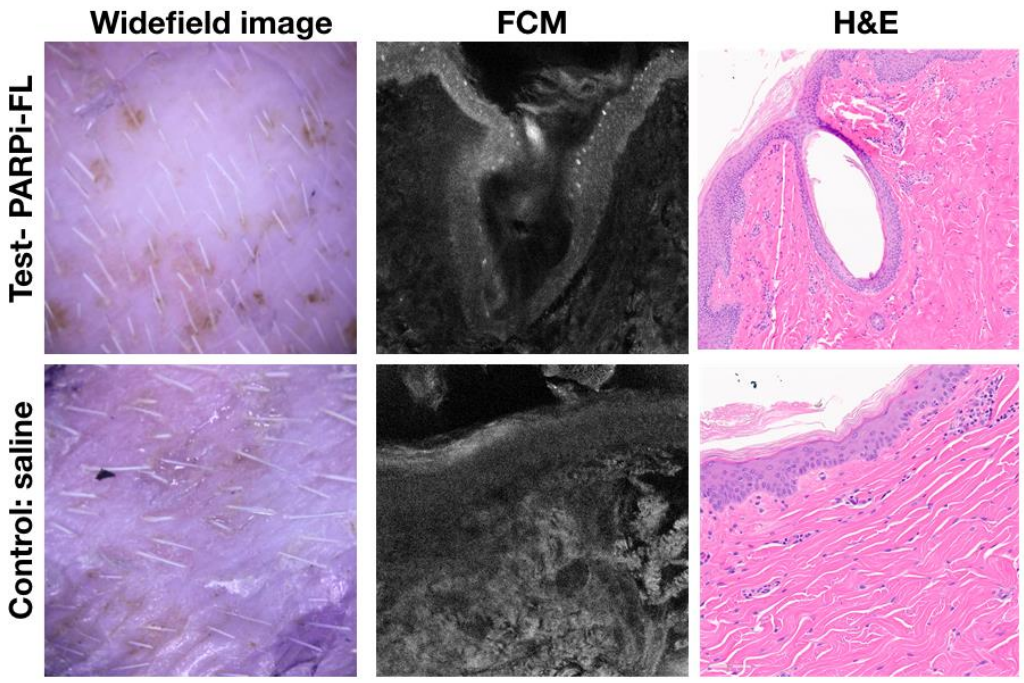

Figure 6. Successful PARPi-FL staining confirmed *in vivo* after topical application in a live pig model

Representative widefield, FCM and H&E demonstrate positive nuclear staining in the basal layer of epidermis in test (PARPi-FL) with absence of nuclear labeling in the control image.

GRAPHICAL ABSTRACT

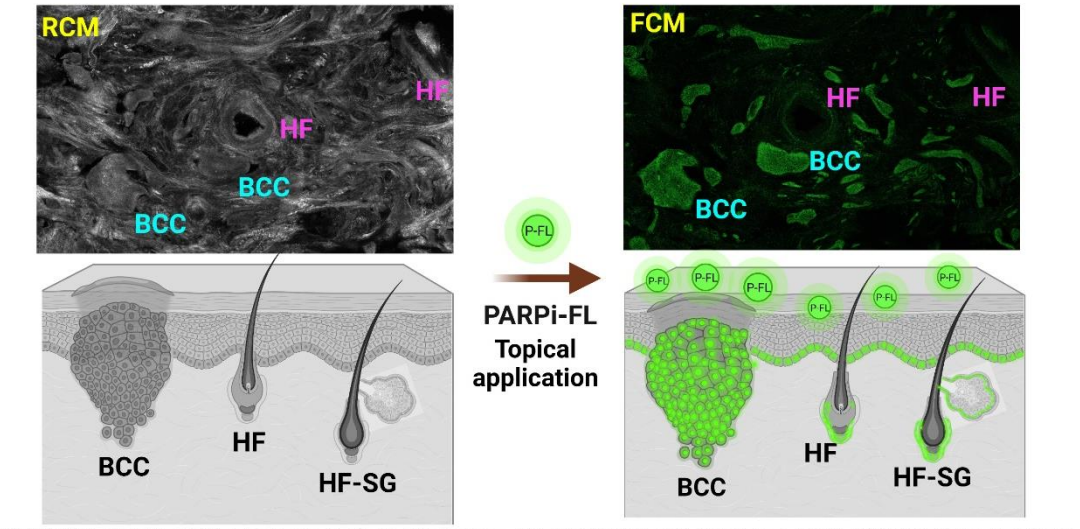

RCM/FCM: reflectance/fluorescence confocal microscopy, HF: Hair Follicle, SG: Sebaceous gland, BCC: basal cell carcinoma

Added nuclear contrast (PARPi-FL) improves BCC visualization and differentiation from mimickers (HF, SG) resulting in higher diagnostic acuracy on RCM+FCM over RCM alone

SUPPLEMENTARY FIGURES

Supplemental Figure 1. A. Protocol for testing PARPi-FL staining, and PARP1-immunofluorescence with H&E in thin sections, B. Protocol for staining whole specimens with PARPi-FL followed by RCM-FCM imaging , C. Protocol for permeability studies in mastectomy specimens in human ex vivo tissue, D. Protocol for PARPi-FL staining in live anesthetized pigs

Supplemental Figure 2. A. Representative example of a thin section annotated by a pathologist, B-D. Representative example of PARP1 IHC along with corresponding H&E in superficial, nodular and infiltrative BCCs, three examples are presented from each subtype. High PARP1 expression is seen in all BCCs, irrespective of subtype, E. Example of heterogenous PARP1 expression

Supplemental Figure 3. A, B. Representative examples of PARPi-FL labeling, PARP1 expression and corresponding H&E in two tissue sections, C. Quantification of average intensity and area positivity at image-level (log transformed data), $p < 0.001$ *for area positivity,* $p < 0.408$ for case-wise intensity, D, E. Quantification of average intensity and area positivity (no log transformation of data) at case-level (C) and image-level (D).

Supplemental Figure 4. A, B. Representative examples of RCM and FCM mosaics that highlight the utility of PARPi-FL in differential labeling of BCC tumors (yellow arrows) and hair follicles (green asterisk), enhancing tumor visualization on FCM, as compared to RCM, C. Representative example demonstrating absence of nuclear staining in nodular-cystic BCC tumor, D. Representative example of infiltrative BCC with heterogenous staining in BCC nests.

Supplemental Figure 5. A. Topical application of PARPi-FL (1 µm for 10 minutes) through saturated gauze in human ex vivo tissue shows positive nuclear staining in epidermis and dermis following

permeation and passive diffusion (DAPI-blue) in pseudo colored images, B. Representative FCM from the in vivo pig experiment (inset). FCM image demonstrates positive nuclear staining in the basal layer of epidermis in test (PARPi-FL) image.

Supplemental Figure 6. A. Fresh normal and BCC tissue from surgical excision immersed in PARPi-FL (1 μM for 30 minutes) or PEG-PBS solution, B, C. Experiments in normal tissue and BCC demonstrate no subsequent effect on histopathological processing and evaluation, and tissue structures, D. Statistical analysis for feature prevalence and agreement indicate matched prevalence of BCC tissues in both groups, and high interrater agreement for BCC diagnosis and staining quality.

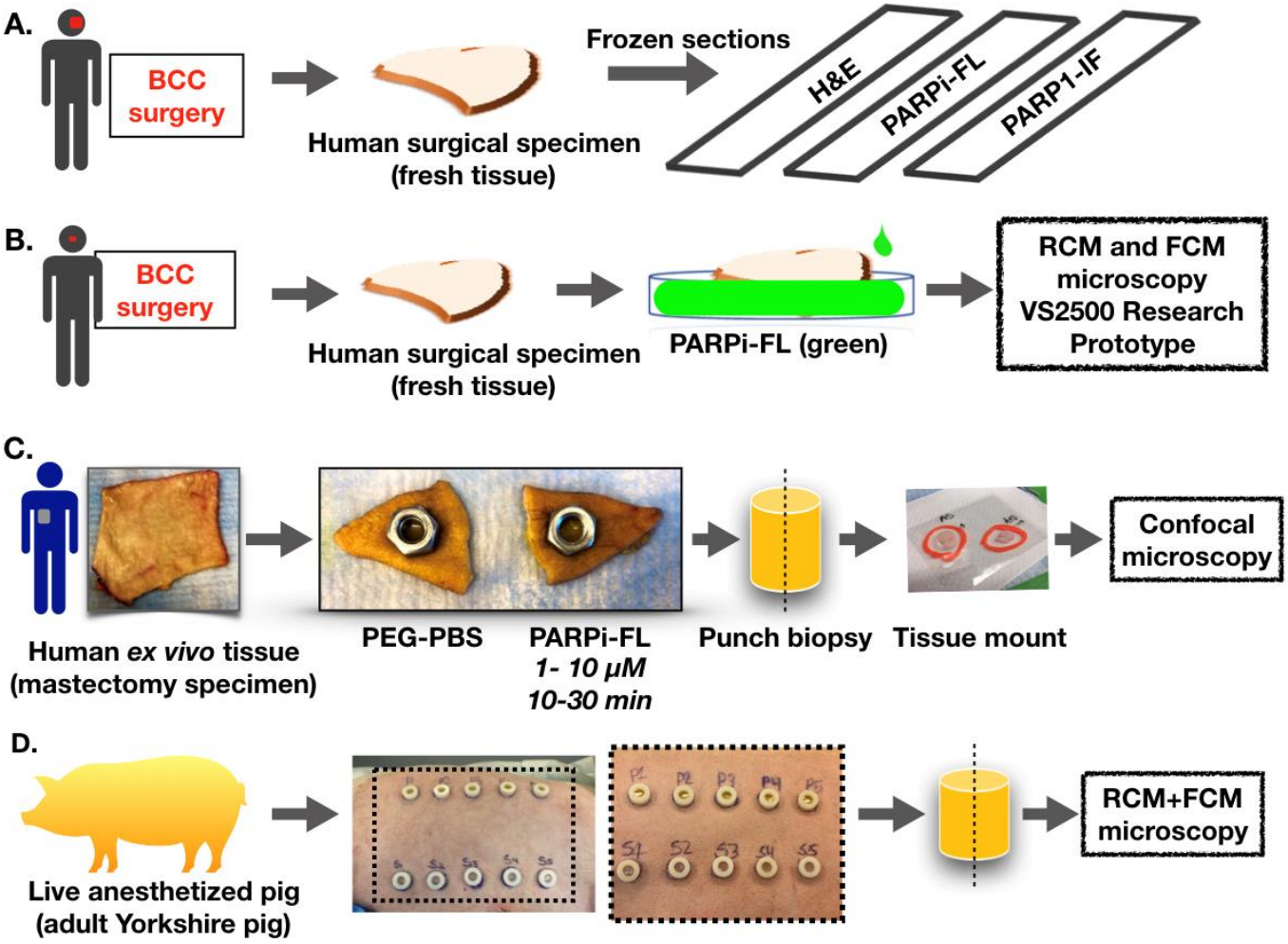

Supplemental Figure 1.

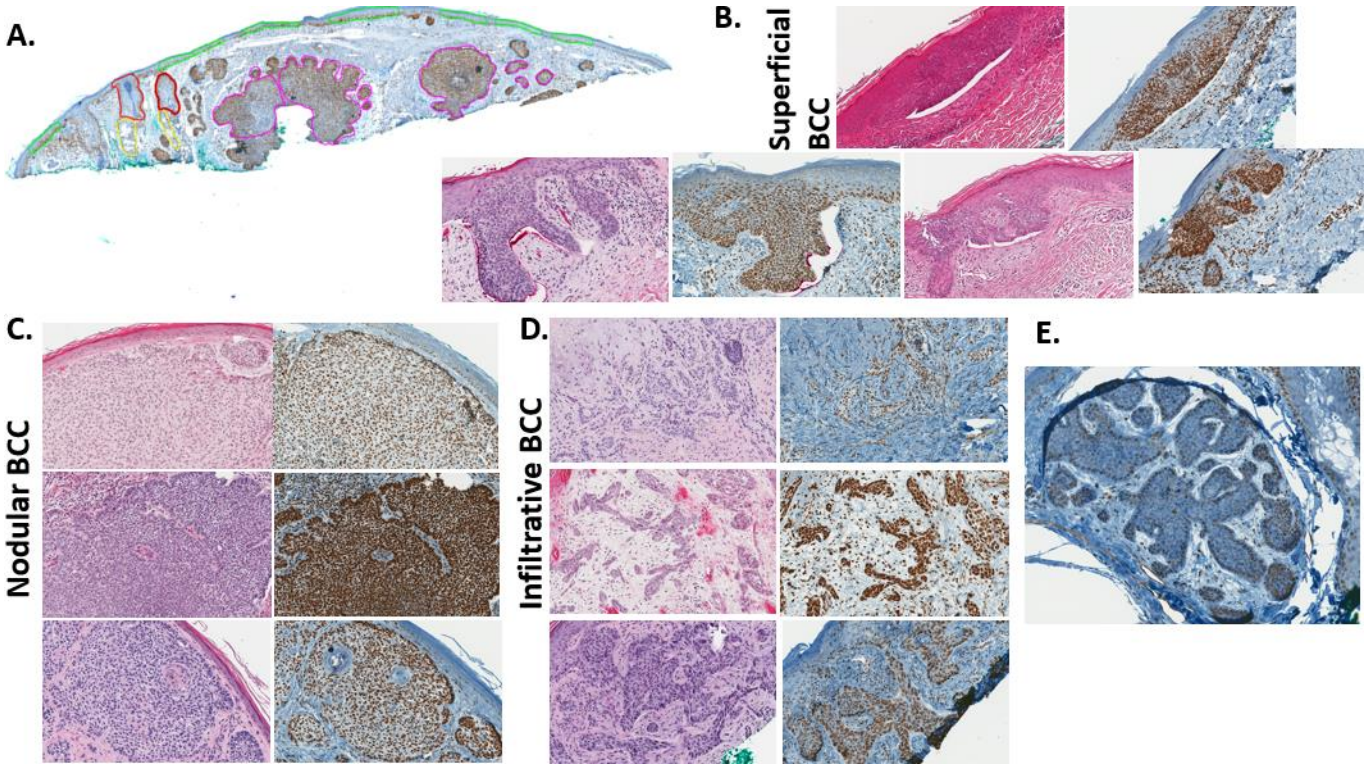

Supplemental Figure 2.

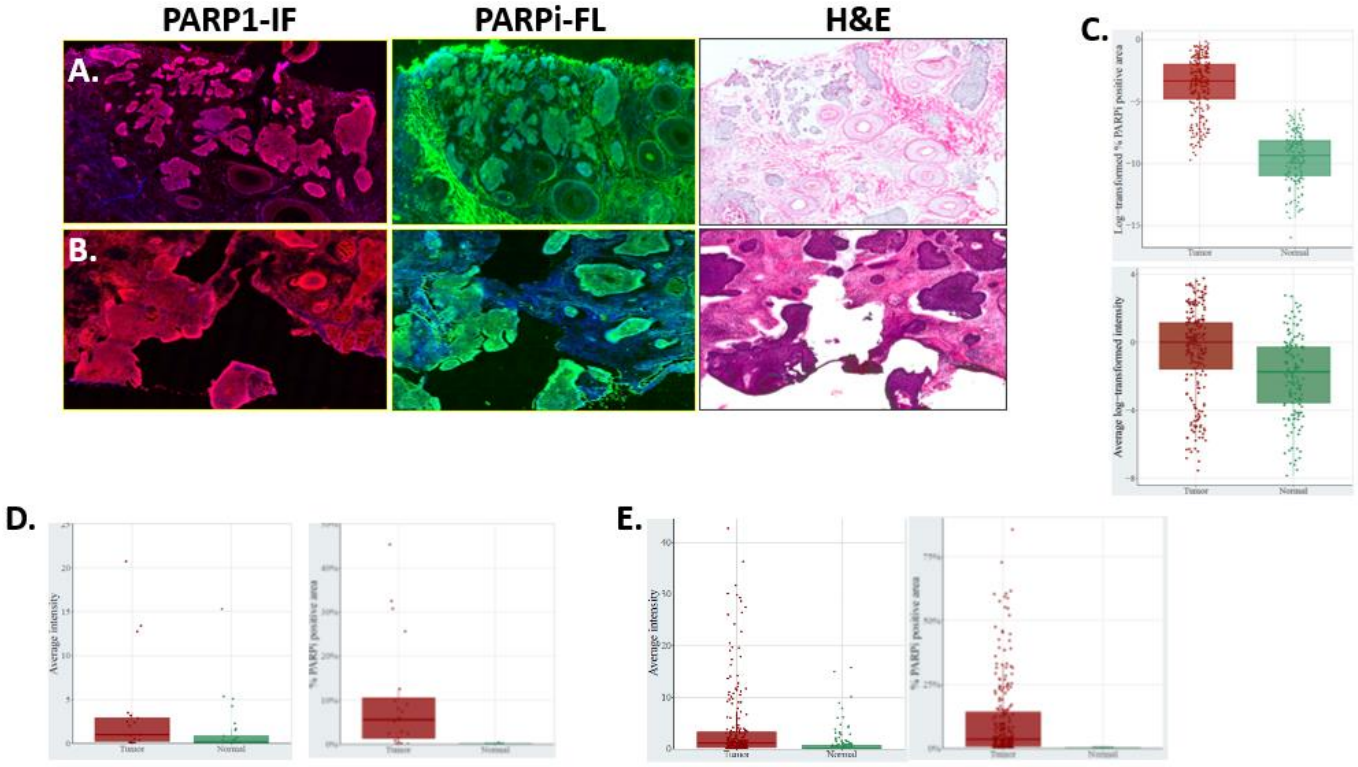

Supplemental Figure 3.

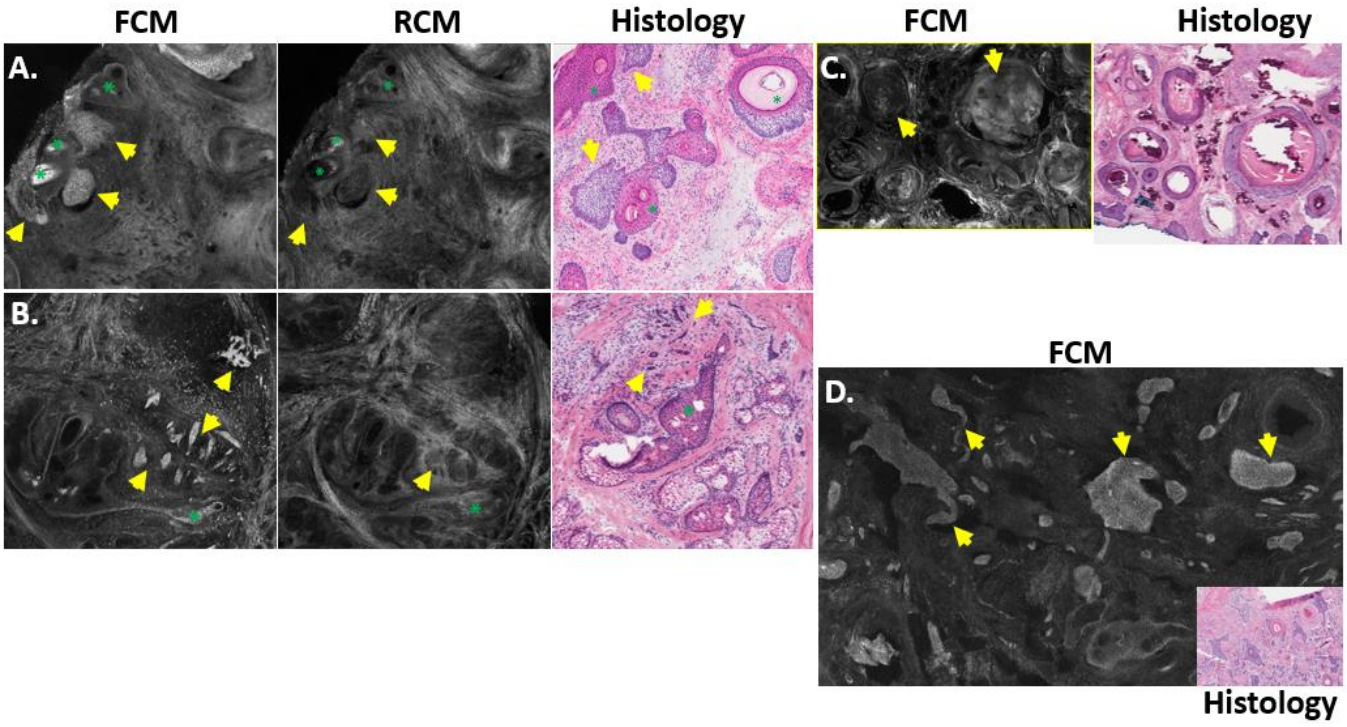

Supplemental Figure 4.

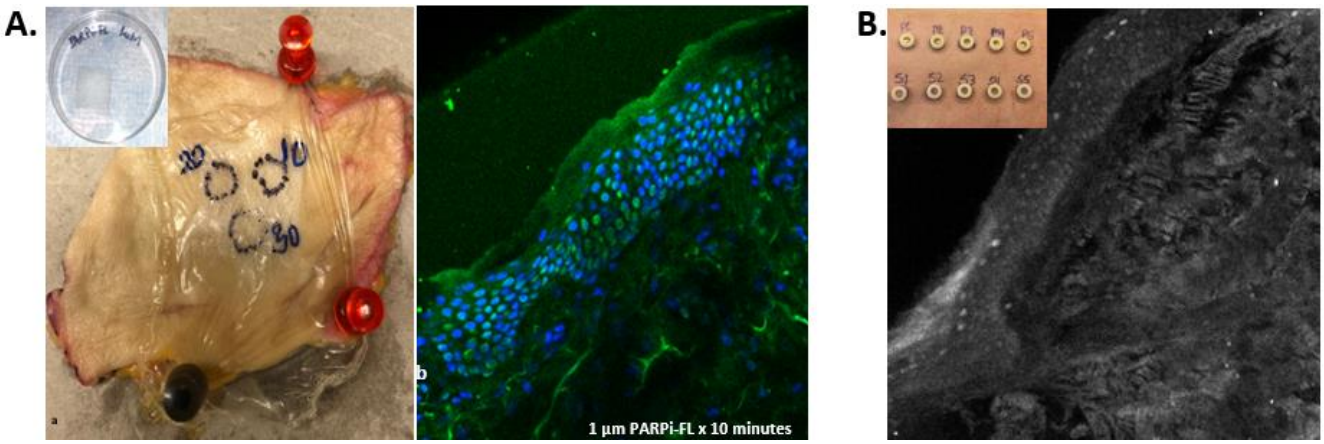

Supplemental Figure 5.

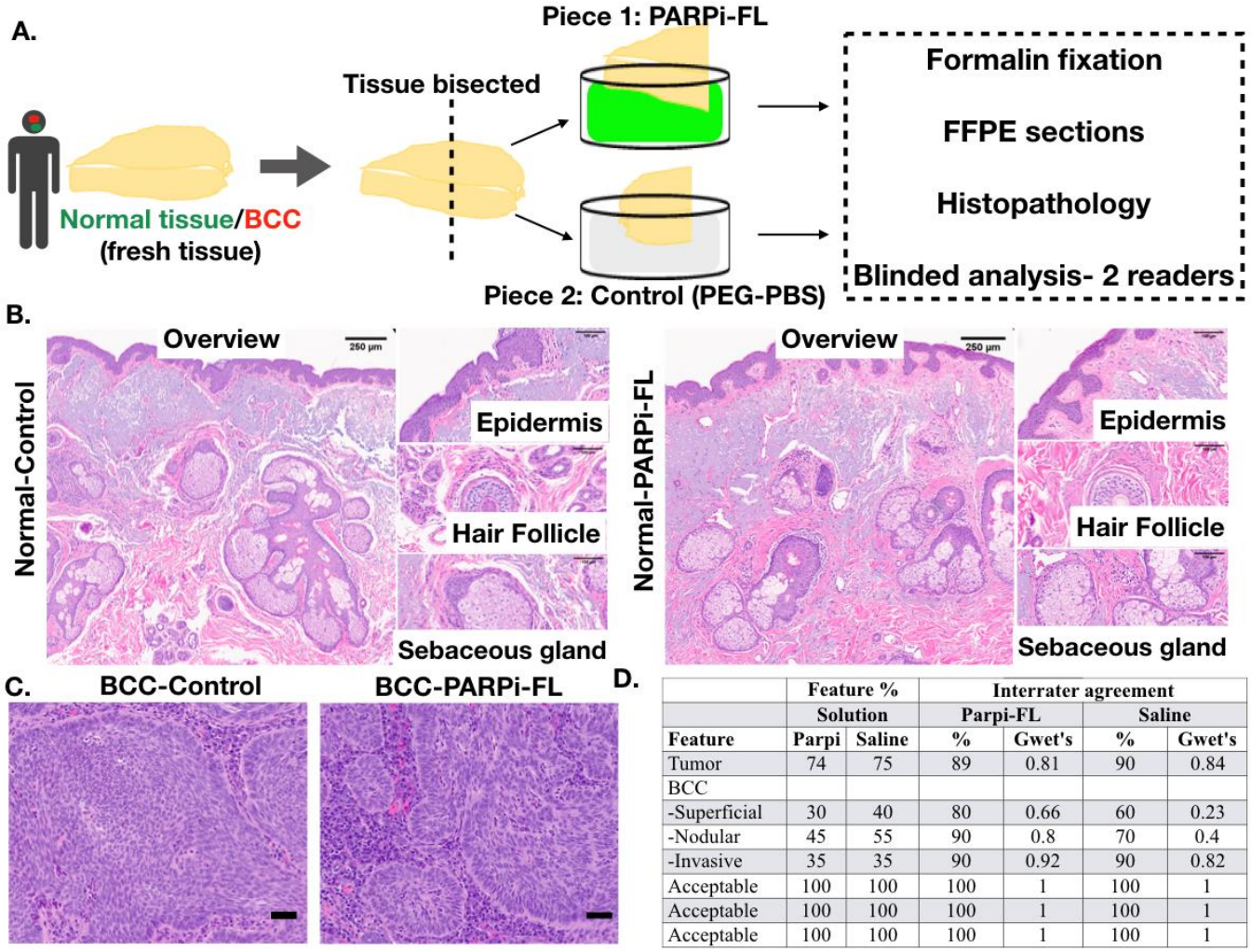

	Feature %		Interrater agreement			
	Solution		Parpi-FL		Saline	
Feature	Parpi	Saline	%	Gwet's	%	Gwet's
Tumor	74	75	89	0.81	90	0.84
BCC						
-Superficial	30	40	80	0.66	60	0.23
-Nodular	45	55	90	0.8	70	0.4
-Invasive	35	35	90	0.92	90	0.82
Acceptable	100	100	100	1	100	1
Acceptable	100	100	100	1	100	1
Acceptable	100	100	100	1	100	1

Supplemental Figure 6.